JACS
JOURNAL OF THE AMERICAN CHEMICAL SOCIETY

ARTICLE

pubs.acs.org/JACS

Layer-by-Layer Assembly and UV Photoreduction of Graphene–Polyoxometalate Composite Films for Electronics

Haolong Li,[†,§] Shuping Pang,[†] Si Wu,[†] Xinliang Feng,[*,†] Klaus Müllen,[*,†] and Christoph Bubeck[*,†]

[†]Max Planck Institute for Polymer Research, Ackermannweg 10, D-55128 Mainz, Germany

[§]State Key Laboratory of Supramolecular Structure and Materials, College of Chemistry, Jilin University, Changchun 130012, China

Supporting Information

ABSTRACT: Graphene oxide (GO) nanosheets and polyoxometalate clusters, $H_3PW_{12}O_{40}$ (PW), were co-assembled into multilayer films via electrostatic layer-by-layer assembly. Under UV irradiation, a photoreduction reaction took place in the films which converted GO to reduced GO (rGO) due to the photocatalytic activity of PW clusters. By this means, uniform and large-area composite films based on rGO were fabricated with precisely controlled thickness on various substrates such as quartz, silicon, and plastic supports. We further fabricated field effect transistors based on the composite films, which exhibited typical ambipolar features and good transport properties for both holes and electrons. The on/off ratios and the charge carrier mobilities of the transistors depend on the number of deposited layers and can be controlled easily. Furthermore, we used photomasks to produce conductive patterns of rGO domains on the films, which served as efficient microelectrodes for photodetector devices.

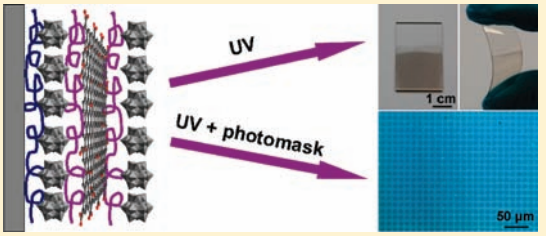

INTRODUCTION

Graphene has inspired great enthusiasm owing to its extraordinary properties including high charge-carrier mobility and optical transparency, as well as flexibility, robustness, and environmental stability.[1−4] It is a promising candidate for a plethora of electronic applications, particularly for thin-film electronic devices.[5−7] Recently, graphene oxide (GO) has emerged as a suitable precursor for large-scale production of graphene materials due to its cost-effective synthesis and superior solution processability.[8,9] Furthermore, oxygen-containing groups on insulating GO nanosheets can be removed by reduction, forming reduced graphene oxide (rGO) with improved electronic properties,[10] which opens an effective route to graphene materials for electronic applications.[11] However, to realize practical rGO-based electronic devices, a precondition is to fabricate high-quality rGO films with large-area uniformity. So far, several methods have been developed to prepare rGO films, such as drop casting,[12] dip coating,[13] spin coating,[14] and vacuum filtration.[15,16] Although these methods succeeded in fabricating some rGO film devices, they suffer from distinct drawbacks: methods such as drop casting, dip coating, and spin coating have difficulties in preparing uniform rGO films with a thickness of several nanometers, and vacuum filtration still needs a film-transfer procedure. Therefore, it is a challenging task to develop a suitable method to overcome the obstacles described above.

Layer-by-layer (LBL) assembly is a widely used method for thin-film fabrication and has been applied to produce multilayer films of charged organic polymers, nanoparticles, and other inorganic materials.[17−19] The LBL method is based on the alternating adsorption of oppositely charged species from dilute solutions onto substrates. It is simple and effective and has the advantage of preparing films with controlled nanometer thickness and uniformity over large areas. It has been reported that GO nanosheets can adsorb on polyelectrolytes to form LBL assembled multilayers,[20,21] owing to their negatively charged surface in aqueous solution.[16] Therefore, it is reasonable to believe that LBL assembly can offer a promising means to fabricate high-quality GO thin films.

When uniform GO thin films are available, the next important step is to convert GO to rGO by suitable reduction methods which re-establish the special electronic properties of graphene. Currently, GO reduction methods mostly rely on chemical and thermal reduction. However, toxic agents such as hydrazine are often used in chemical reduction processes, and the high-temperature treatment of thermal reduction is not suitable for plastic electronics. For comparison, photoreduction, as a mild and environmentally friendly method, is now receiving attention as an alternative approach for producing rGO.[22−26] Furthermore, photoreduction can be easily triggered by light, allowing researchers to pattern circuit-like structures such as those obtained in well-established photolithography, which is very appealing for microelectronic industries.[24] We have reported that a Keggin-type polyoxometalate cluster, $H_3PW_{12}O_{40}$ (PW), can act as an effective photocatalyst to reduce GO nanosheets in water solution under UV irradiation, yielding rGO with good electrical conductivity.[26] In principle, this type of photoreduction process can also be performed in thin films consisting of GO

Received: February 20, 2011
Published: May 16, 2011

Scheme 1. Schematic Illustration of the Fabrication Procedure of rGO-PW Multilayer Films, Which Involves the LBL Assembly of GO Nanosheets and PW Clusters Using Cationic Polyelectrolytes PEI and PAH as Electrostatic Linkers, and a Subsequent in Situ Photoreduction To Convert GO to rGO

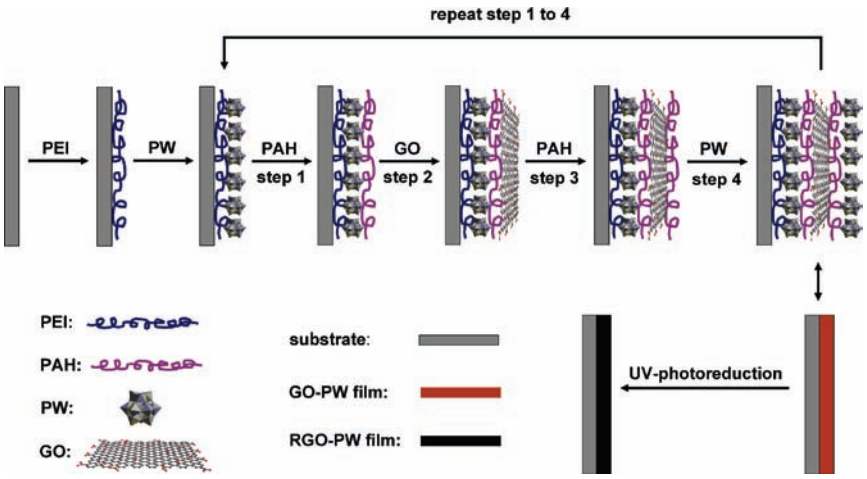

nanosheets and PW clusters. On the other hand, the anionic surface of polyoxometalate clusters allows us to incorporate them into polyelectrolyte films by electrostatic attraction.[27−31] Therefore, we envision that GO and PW can be co-assembled into multilayer films via LBL alternating deposition.

In this work, we demonstrate the fabrication of high-quality rGO composite films by means of the LBL assembly procedure. GO nanosheets and PW clusters were incorporated in multilayer films, and a subsequent in situ photoreduction procedure converted GO to rGO due to the photocatalytic activity of PW (Scheme 1). In this way, ultrathin and large-area rGO films were easily and reproducibly prepared with several nanometers thickness and uniform morphology. Thin-film field effect transistors (FETs) based on these graphene films were fabricated, showing typical ambipolar characteristics and good transport properties for both electrons and holes. The on/off ratios and the mobilities of the transistors can be easily tailored by varying film thickness and thus the number of deposited layers. Furthermore, we used photomasks to produce conductive patterns of rGO domains with the size down to several micrometers, which were directly generated on the initial GO-PW composite films. Importantly, the rGO patterns can serve as microelectrodes, e.g., for photodetector devices.

RESULTS AND DISCUSSION

Layer-by-Layer Assembly of GO-PW Films. GO was oxidized from natural graphite flakes by a modified Hummers method.[32] The pH value of GO solution is ∼7, and its zeta potential is about −40 mV, which means that GO nanosheets are negatively charged.[16] GO and PW both show characteristic absorptions in the UV−vis region, as presented in Figure 1A. Two absorption bands of GO appear at 230 and 300 nm respectively, while the well-known ligand-to-metal charge-transfer (LMCT) transition band of PW is located at 260 nm with an extinction coefficient of $\sim 7.5 \times 10^4\ M^{-1}cm^{-1}$. Therefore, it is easy to monitor the formation of GO-PW multilayer films by UV−vis spectroscopy, according to the film absorbance at the characteristic absorption bands of GO and PW.

In the LBL assembly process, electrostatic interaction is the driving force owing to the negatively charged surface of GO nanosheets and PW clusters in water solution. First, the substrates were modified by a PEI/PW double layer as precursor films, and then different numbers of PAH/GO/PAH/PW layers were deposited on the modified substrates to construct GO-PW multilayer films, in which GO nanosheets and PW clusters are linked by PAH layers (Scheme 1). In such a film structure, the PW layers exist on both sides of the GO layers. This design aims to realize an effective interaction between oxygen-containing groups on GO nanosheets and PW clusters, which is favorable for the electron transfer from photoexcited PW to GO, thus realizing an efficient reduction of GO in the subsequent PW-assisted photoreduction process. Figure 1B displays the UV−vis absorption spectra of $(PAH/GO/PAH/PW)_n$ multilayer films (with n = 1−6) assembled on a PEI/PW precursor film on quartz substrates. The absorption of the films increases systematically with the layer number n, which is evidence for the subsequent deposition of GO and PW components. When monitoring the detailed absorption variation during a PAH/GO/PAH/PW assembly process, the absorbance of films is found to increase after each deposition processes of GO and PW, implying that the two components are indeed assembled into the films (see Figure S1 in the Supporting Information (SI)). PAH does not absorb above 200 nm. Therefore, its presence in the films is not reflected in the absorption spectra. The absorbance values for $(PAH/GO/PAH/PW)_n$ multilayer films with n = 1−6 at 230, 260, and 300 nm are plotted as function of the layer number n, as shown in the inset of Figure 1B. Apparently, the absorbance varies linearly with n at all three wavelengths, which reveals a constant increase in the total amount of GO and PW adsorbed in the films after each deposition cycle of PAH/GO/PAH/PW layer. Furthermore, the film fabrication is highly reproducible. It is noted that the absorption variation of four separately prepared $(PAH/GO/PAH/PW)_6$ films shows a consistent linear relationship with layer numbers, and the fitted plots overlap well, as revealed in Figures S2−S4 (SI). Such a reproducible production guarantees the advantage of the LBL assembly method in precisely controlling the film structure

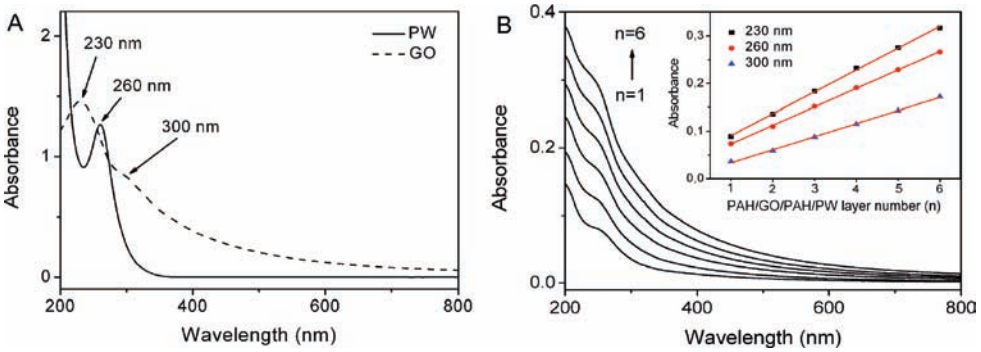

Figure 1. (A) UV−vis absorption spectra of an aqueous 0.05 mg/mL PW solution (black line, PW concentration is 1.7×10^{-5} M) and an aqueous 0.05 mg/mL GO solution (red line). (B) UV−vis absorption spectra of LBL-assembled $(PAH/GO/PAH/PW)_n$ multilayer films with layer number n = 1−6 on a quartz substrate, which was modified before by a PEI/PW precursor film. The blank substrate was used as reference. The curves, from bottom to top, correspond to n = 1−6. Inset: plots of the absorbance values at 230, 260, 300 nm as a function of the layer number n.

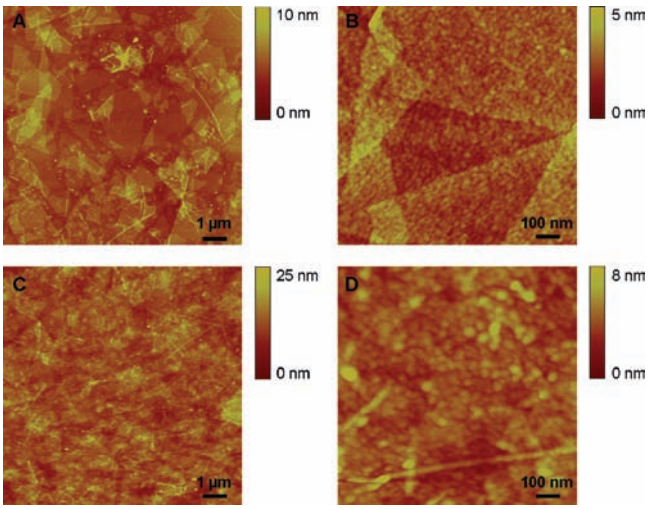

Figure 2. AFM images of a $(PAH/GO/PAH/PW)_1$ film (A,B) and a $(PAH/GO/PAH/PW)_6$ film (C,D), both on PEI/PW precursor film-modified silicon substrates, which contain 300 nm thermal oxide.

and thickness, which fulfills the requirement for electronic applications.

Based on the UV−vis spectra, it is possible to calculate the surface coverage density Γ of PW clusters in each PAH/GO/PAH/PW layer by using the relation $\Gamma = (N_A A_\lambda)/2\varepsilon_\lambda$, where N_A is Avogadro's constant (6.02×10^{23} mol^{-1}), A_λ is the absorbance of PW in a PAH/GO/PAH/PW layer at a given wavelength λ, and ε_λ is the isotropic molar extinction coefficient of PW at λ.[27,33] In the current calculation, the relative maximum λ_{max} of the LMCT transition band of PW at 260 nm is used. From Figure S1 in the SI, we can obtain the A_{260} value (∼0.01) from the variation of film absorbance resulting from the adsorption of one layer of PW in PAH/GO/PAH/PW film. This value is divided by 2 to give a surface density for a single layer of PW, since the films were deposited on both sides of quartz substrate. ε_{260} of PW is $\sim 7.5 \times 10^4$ M^{-1} cm^{-1}, as mentioned above. By using these parameters, the average PW surface coverage density of 4×10^{13} clusters/cm^2 is obtained, which corresponds to an average area per PW of 2.5 nm^2. Assuming that a single PW cluster has an area of approximately 0.8 nm^2 due to its T_d-symmetric spherical shape and 1 nm diameter,[34] the average surface coverage of PW is calculated to be ∼32%. It has been reported that a high ionic strength condition can screen the electrostatic repulsive interaction between small polyoxometalate clusters (1−2 nm in diameter), enabling the clusters to come into close contact, which eventually gives rise to multilayer coverage.[31] In principle, multilayer coverage will induce a larger surface roughness which is unfavorable for the electronic device fabrication. Therefore, we carried out the electrostatic deposition of PW in its pure aqueous solution without additional salts, which is a typical low ionic strength condition and effectively avoids the formation of multilayer coverage.

The surface morphology of the GO-PW films was characterized by atomic force microscopy (AFM) measurement. The AFM image of a $(PAH/GO/PAH/PW)_1$ film on silicon substrate is shown in Figure 2A. Obviously, the film is covered by a monolayer of GO nanosheets with a high surface coverage, although some nanosheets overlap at the edge regions. The root-mean-square deviation value of the surface roughness (R_q) for the whole region in Figure 2A (10×10 μm^2) is 1.17 nm, indicating a very smooth surface of the film. Furthermore, the smooth surface morphology is uniformly distributed over the whole region of a large-area film (1 cm × 2 cm), based on comparing the AFM images of different positions on the film. Such a uniform morphology is an intrinsic advantage of the LBL assembly method, which further determines the excellent electronic property of the films, as discussed below. The magnified AFM image of a $(PAH/GO/PAH/PW)_1$ film (Figure 2B) shows that small PW domains exist uniformly on the surface of GO nanosheets, which are several square nanometers large and appear 2−3 nm higher than their surroundings. The domains are ascribed to the PW clusters adsorbed on PAH chains.[31] The uniform adsorption of PW clusters endows the $(PAH/GO/PAH/PW)_1$ film a very smooth surface morphology, as the R_q value of the 1×1 μm^2 area in Figure 2B is only 0.59 nm. On the other hand, the AFM images of $(PAH/GO/PAH/PW)_6$ films show a tight stacking morphology of multilayer GO nanosheets (Figure 2C). Meanwhile, the area of PW domains increased to more than 10 nm^2, and the film roughness also become slightly larger (see Figure 2D). Increased roughness is commonly observed for the first few layers in LBL-assembled multilayer films, due to a substrate effect.[31] Even so, the roughness measurement of $(PAH/GO/PAH/PW)_6$ films still shows a rather smooth surface: the R_q values of the 10×10 μm^2 area in Figure 2C and the 1×1 μm^2 area in Figure 2D are 2.46 and

dx.doi.org/10.1021/ja201594k | J. Am. Chem. Soc. 2011, 133, 9423–9429

0.90 nm, respectively, which are only 2 times larger than that of the $(PAH/GO/PAH/PW)_1$ film. A large-area SEM image of $(PAH/GO/PAH/PW)_6$ films further confirms its smooth surface (see Figure S5, SI). The low roughness between 1 and 2 nm of the GO-PW multilayer films is certainly advantageous for the fabrication of large-area thin-film electronic devices. According to the height profile, the thickness of $(PAH/GO/PAH/PW)_6$ film is approximately 12 nm (see Figure S6, SI). By subtracting the thickness of $(PAH/GO/PAH/PW)_1$ film from that of $(PAH/GO/PAH/PW)_6$ film and dividing the result by 5, the average effective thickness per PAH/GO/PAH/PW is estimated to be 2 nm. This value is smaller than the total thickness of 3.9 nm expected for an ideal multilayer on the basis of literature data: one layer of PW cluster (1 nm),[34] one layer of GO nanosheet (0.9 nm),[26] and two layers of PAH (2 nm).[30] We attribute the difference to an inadequate occupancy of PW clusters in each layer, because its surface coverage density is only 32%, as discussed above.

UV Photoreduction of GO-PW Films. GO-PW multilayer films were prepared on different hydrophilic substrates, such as quartz and oxygen plasma-treated flexible PET substrates,[35] by means of the LBL assembly method described above, as shown in Figure 3A,C. However, these GO-PW films are insulating due to the nature of the GO nanosheets.[8−11] An in situ photoreduction of the films was employed to convert the GO nanosheets into conductive rGO. In the photoreduction procedure, the GO-PW multilayer films were irradiated by a 100 W high-pressure mercury lamp (combined with filters to provide $\lambda > 280$ nm) to oxidize the organic polyelectrolytes and reduce the GO nanosheets by using the photocatalytic activity of PW clusters.[26]

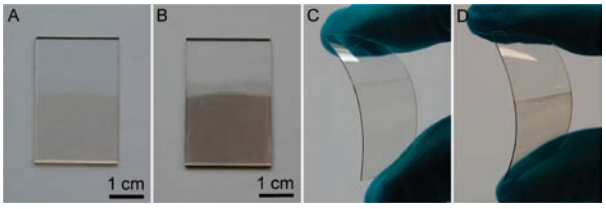

Figure 3. Optical images of a $(PAH/GO/PAH/PW)_6$ multilayer film prepared on a quartz substrate before (A) and after (B) 6 h of UV photoreduction and on a flexible PET substrate before (C) and after (D) 6 h of UV photoreduction. Both substrates are coated first by a PET/PW precursor film.

The color of the films gradually turned from light brown to dark (Figure 3B,D), suggesting the successful formation of rGO.

Figure 4A shows the UV−vis spectra of the films in the whole UV−vis region. The absorbance of the films gradually increases with the irradiation time of UV light, and its value rises up to a plateau after about 6 h, which means that the photoreduction reaches a saturation state (Figure 4A inset). AFM characterization indicates that the reduced GO-PW films possess the same surface morphology as the original film, suggesting the mild photoreduction conditions of the present method. A detailed comparison of the film morphologies before and after photoreduction will be presented below. In contrast to our observation, Huang et al. reported that the photoreduction can be dominated by a photothermal heating effect, which causes significant expansion of the thickness of GO films, about 10 times compared to the original films, and thus the film morphology was unavoidably changed.[24] However, in our work, the samples were kept at room temperature due to the weak heating effect of UV light and the use of an airflow cooling system. Therefore, the photoreduction process should be determined by a photochemical reaction, with the same mechanism as was presented for the PW-assisted photoreduction in solution.[26] The photocatalytic activity of PW is similar to that of semiconductor nanoparticles, such as TiO_2 nanoparticles. Under the irradiation of UV light, the O→W charge-transfer band in the PW cluster is excited, which leads to electron−hole separation.[36] The excited PW clusters can play the role of both oxidant and reductant. It has been reported that photoexcited titania nanosheets can oxidize PAH in LBL films,[25] from which a similar process can be concluded in the present GO-PW composite films: PAH is oxidized by excited PW. On the other hand, the electrons trapped in the cage-type structure of excited PW clusters transfer to GO nanosheets, resulting in the reduction of GO. In the whole photoreduction process, PW acts as photocatalyst and electron relay.[36,37] This process can be described as

$$PW + h\nu \rightarrow PW(h + e)$$

$$PW(h + e) + PAH \rightarrow PW(e) + \text{oxidized PAH}$$

$$PW(e) + GO \rightarrow PW + rGO$$

Similar mechanisms have also been proposed earlier in the systems of GO and other semiconductor nanoparticles such as

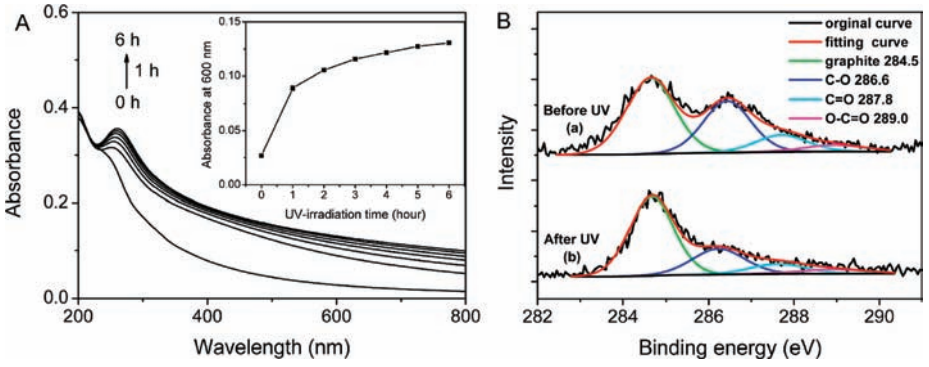

Figure 4. (A) UV−vis spectra of a $(PAH/GO/PAH/PW)_6$ multilayer film prepared on a PEI/PW precursor film-modified quartz substrate after various irradiation times of the UV-photoreduction process. The inset shows absorbance values at 600 nm as a function of the irradiation time. (B) C 1s XPS spectra of a $(PAH/GO/PAH/PW)_6$ film on a PEI/PW precursor film-modified quartz substrate before (curve a) and after (curve b) 6 h of UV photoreduction.

dx.doi.org/10.1021/ja201594k | J. Am. Chem. Soc. 2011, 133, 9423–9429

TiO_2 and ZnO.[22,23] It is worth noting that the photoreduction was efficient even in air atmosphere, because the oxygen in air can oxidize the photoexcited PW to ground state and lower the photocatalytic effect.[36] Here, we believe that the tight interaction of GO layer, PW layer, and PAH layer in LBL films can prevent PW clusters from being exposed to external oxygen, thus leading to an efficient photoreduction process. It should be noted that the photoreduction cannot take place without PW in the films. In our previous work using PW to photoreduce GO in water solution, we also found that the photoreduction did not occur if PW was not added into the solution.[26] Therefore, the photocatalytic activity of PW is crucial for GO reduction in the present work.

X-ray photoelectron spectroscopy (XPS) was employed to analyze the compositional change of carbon atoms in different chemical states of GO-PW films before and after photoreduction. Figure 4B shows the C 1s XPS spectra before and after UV irradiation. Four types of carbon with different chemical states are observed, which appear at 284.5 (graphite, C−C/C═C), 286.6 (C−O), 287.8 (C═O), and 289.0 eV (O−C═O), respectively. Both XPS spectra were fitted to evaluate the relative areas of the peaks. The results are shown in Table 1. Inspection of Figure 4B and Table 1 shows that the relative areas of all peaks corresponding to oxygen-containing groups decreased when the film underwent a 6 h photoreduction. In particular, the percentage of the C−O group greatly decreased from initial 41.1% to 20.9%, which suggests that many oxygen-containing moieties were eliminated by photoreduction. Meanwhile, the content of C−C/C═C group increased from to 44.8% to 65.6%, indicating that significant sp^3/sp^2-hybridized carbon structures were restored.

Table 1. Fitting Results of the C 1s XPS Spectra Shown in Figure 4B of the $(PAH/GO/PAH/PW)_6$ Film before and after 6 h of UV Photoreduction

		relative area (%)	
type of carbon	binding energy (eV)	before photoreduction	after photoreduction
graphite	284.5	44.8	65.6
C−O	286.6	41.1	20.9
C═O	287.8	9.9	9.7
O−C═O	289.0	4.2	3.8

The electrical conductivity measurement of rGO also provides a means to judge the degree of reduction of GO. After 6 h of photoreduction, photoreduced rGO-PW films of $(PAH/GO/PAH/PW)_1$ and $(PAH/GO/PAH/PW)_6$ show conductivity of about 10 and 120 S m^{-1}, respectively. Apparently, these values are comparable to those of the rGO films produced by chemical methods,[38] highlighting the efficient conversion of GO to rGO in this work.

Electronic Properties of rGO-PW Films. Electronic applications represent one of the most important areas of research in the field of rGO-based materials.[9−11] For this reason, the fabrication of rGO-based transistors has attracted particular attention, requiring the preparation of high-quality and ultrathin rGO films with uniform morphology on large-area substrates.[11] The rGO-PW composite films fulfill these needs. To demonstrate the transport performance of these graphene films, we fabricated FET devices based on $(PAH/GO/PAH/PW)_1$ and $(PAH/GO/PAH/PW)_6$ films. A scheme and optical images of typical FET devices are depicted in Figure 5A,B. Both films were deposited on silicon substrates which had a 300 nm thermal oxide layer. Au electrodes with a channel width of 400 μm and a channel length of 20 μm were thermally evaporated on the films as source and drain electrodes. The silicon substrate was used as gate electrode, and the thermal oxide layer on the silicon surface acted as insulator layer. Both FET devices exhibit ambipolar field effect, which is typical for graphene transistors[15]

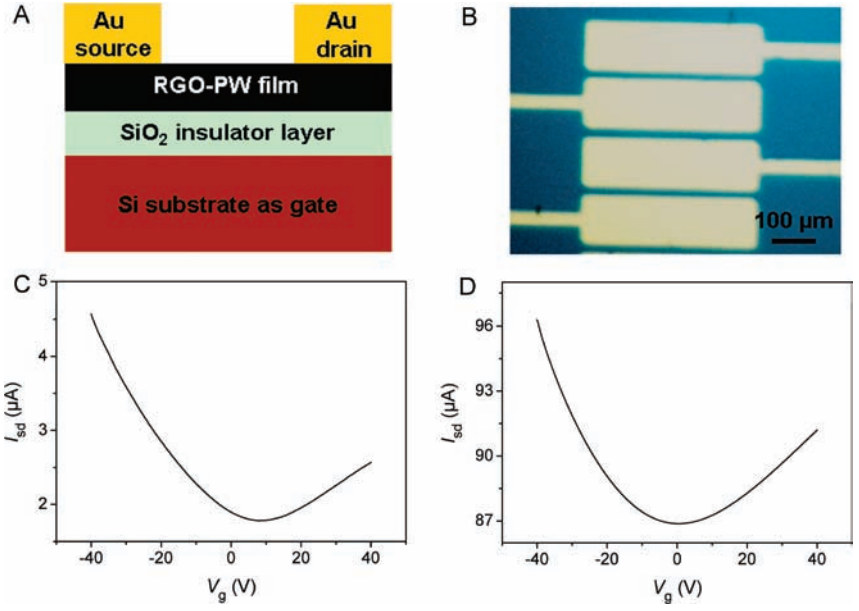

Figure 5. (A) rGO-PW film-based FET devices (cross section). (B) Optical microscope image of the actual device (top view). The blue part is the surface of the rGO-PW films. The Au electrodes appear bright. (C,D) $I_{ds}-V_g$ curves of the FET devices fabricated on a $(PAH/GO/PAH/PW)_1$ film (C) and a $(PAH/GO/PAH/PW)_6$ film (D). Both samples were prepared on PEI/PW precursor film-modified silicon substrates with 300 nm thermal oxide and underwent 6 h of UV photoreduction. V_{sd} = 10 V.

dx.doi.org/10.1021/ja201594k |J. Am. Chem. Soc. 2011, 133, 9423–9429

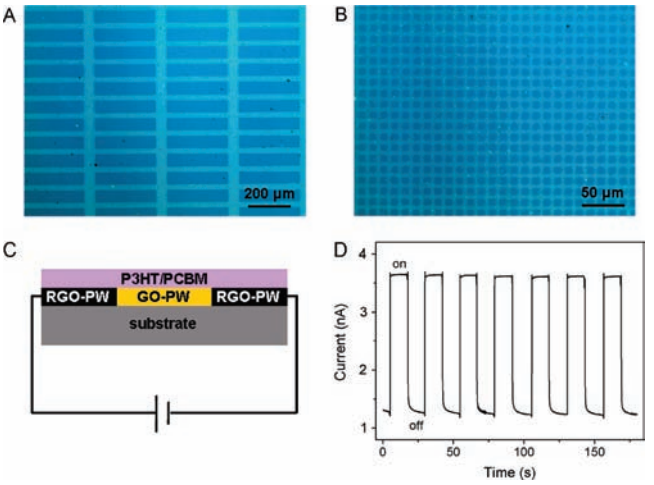

Figure 6. (A,B) Optical microscope images of reduced patterns on $(PAH/GO/PAH/PW)_6$ multilayer films on PEI/PW precursor film-modified silicon substrates with 300 nm thermal oxide. The patterns were made by 6 h of UV photoreduction using different photomasks. (C) Cross-section of the photodetector device using conductive patterns of rGO-PW film as microelectrodes and the photoswitching material P3HT/PCBM, which is spin-coated on the patterns. (D) Photocurrent response of the photodetector based on the conductive patterns in part A versus time under chopped irradiation, at a bias voltage of 10 V.

(Figure 5C,D). Electron and hole mobilities can be extracted from the linear regime of the transfer characteristics, using the equation $\mu = [(\Delta I_{sd}/\Delta V_g)(L/W)]/C_{ox}V_{sd}$,[6] where L and W are channel length and width, C_{ox} is the capacitance of silicon oxide gate (which is 1.27×10^{-8} F/cm^2 for a 300 nm thick silicon oxide), V_{sd} is the source-drain voltage (which is 10 V in the present work), I_{sd} is the source-drain current, and V_g is the gate voltage. $\Delta I_{sd}/\Delta V_g$ is the transconductance or the slope of the transfer curve in the linear regime. From the $I_{sd}-V_g$ curves, we can derive hole and electron mobility values of $\mu_h = 0.03$ and $\mu_e = 0.01$ cm^2 V^{-1} S^{-1} for the $(PAH/GO/PAH/PW)_1$ film device, and $\mu_h = 0.15$ and $\mu_e = 0.06$ cm^2 V^{-1} S^{-1} for the $(PAH/GO/PAH/PW)_6$ film device. It has been reported that adsorbing small molecules such as water and oxygen on rGO FET devices results in hole-dominated transporting.[39,40] In our work, the cage-type structure of PW can trap electrons,[36] which probably causes the rGO-PW FET devices to exhibit a hole-dominated transport behavior. The on/off ratio, which is defined as the ratio of maximum and minimum values of I_{sd}, of the $(PAH/GO/PAH/PW)_1$ film device is ~2.0, and that of the $(PAH/GO/PAH/PW)_6$ film device is ~1.1. These values are similar to those reported for rGO films prepared by chemical or thermal reduction methods.[15,39−41] Thus, it is evident that the electronic transport properties of the as-fabricated FET devices greatly depend on the film thickness: the devices with thicker films exhibit a higher mobility and a lower on/off ratio. As discussed above, the thickness of the rGO-PW film can be precisely adjusted by controlling the number of deposited layers. This feature makes our method well superior for the fabrication of rGO-based FET devices with tailorable properties. Furthermore, we note that all the FET devices distributed on a 1 cm × 2 cm large-area film work well and exhibit similar transport properties, which we attribute to the high uniformity of the films.

Besides their use as active components in transistors, graphene films have another important application as electrode material.[11] Although several methods for film preparation, such as spin coating, dip coating, and vacuum filtration involving a chemical or thermal reduction procedure, have been developed to fabricate rGO-based electrodes, the direct fabrication of patterned thin-film electrodes still remains difficult, due to the nonselective feature of chemical or thermal reduction.[11] Normally, a further tedious lithographic procedure is needed to accomplish the pattern formation.[42,43] On the other hand, a photoreduction strategy has the advantage to reduce GO in selected patterned areas only when a photomask is utilized.[24] Herein, we placed copper grids on the GO-PW films as photomasks and realized a selected-area irradiation of UV light. In this way, well-ordered conductive rGO rectangles of micrometer size were directly patterned on the films. The optical images of the patterns are shown in Figure 6A,B. Moreover, AFM images of the patterns in SI Figure S7 demonstrate that the reduced and nonreduced domains possess the same surface morphology. This suggests that the present UV-photoreduction-assisted patterning procedure, without any additional etching process, is mild and does not affect the intrinsic structure of the films.

To demonstrate the application of the as-fabricated rGO patterns, we employed them as microelectrodes for photodetector devices by spin-coating a thin film of the blend of poly(3-hexylthiophene) (P3HT) and 1-(3-methoxycarbonyl)propyl-1-phenyl[6,6]C_{61} (PCBM) on the patterns. P3HT/PCBM blend is a classical active component for bulk heterojunction solar cells, which shows a strong photoinduced charge separation performance.[44] Here, we used them as photoswitching materials in the photodetectors. The scheme of the photodetector is illustrated in Figure 6C. The detector is typically composed of two adjacent rGO patterns as electrodes with the bridging P3HT/PCBM film between them. The photoswitching property of the photodetector based on $(PAH/GO/PAH/PW)_6$ films was investigated and exhibited a well repeatable photocurrent response, with an on/off ratio of ~3, under the switching stimulus of an external light source (see Figure 6D).

CONCLUSION

We have developed a facile and environmentally benign method for the fabrication of rGO composite films, which combines LBL assembly and in situ photoreduction procedures. In this method, GO nanosheets and PW clusters are alternately deposited on substrates via electrostatic adsorption, followed by a UV-photoreduction procedure that converts GO to conductive rGO due to the photocatalytic role of PW.[26] By this means, large-area, smooth, and uniform rGO-PW composite films can be easily fabricated on various substrates like quartz glass, silicon wafers, and flexible polymers. We prepared FET devices based on the composite films. The devices show ambipolar characteristics and tunable charge-carrier mobilities which can be adjusted by controlling the number of deposited rGO layers. Furthermore, we used photomasks to prepare photoreduced, conductive rGO patterns on the films and demonstrate their function as microelectrodes for photodetectors. Taking into account the simple and efficient fabrication procedure, this work offers a new strategy to prepare ultrathin rGO films with high quality and uniformity, which facilitates application of the intriguing electronic properties of graphene. Moreover, the performance of rGO devices prepared by our method can be further improved by using the large-sized GO nanosheets reported recently, which exhibit much higher electrical conductivities and carrier mobilities.[45,46] On the other hand, it can be envisioned that multifunctional rGO devices can

be achieved by incorporating different functional polyoxometalates: for example, the integration of magnetic polyoxometalate clusters into rGO films can lead to new molecular memory devices.[47] In addition, the construction of logic-gate devices with dual optical and electrical output functions will become possible by a rational combination of the luminescent property of polyoxometalate clusters with the electric response of rGO films.[48]

■ ASSOCIATED CONTENT

Supporting Information. Detailed experimental procedures; UV−vis absorption spectra of the detailed LBL assembly process of a $(PAH/GO/PAH/PW)_1$ multilayer film (Figure S1); plots of the absorbance values of four separately prepared $(PAH/GO/PAH/PW)_n$ multilayer films with $n = 1-6$ at 230, 260, and 300 nm as a function of n (Figures S2−S4); SEM images of $(PAH/GO/PAH/PW)_6$ films (Figure S5); AFM images and height profiles of the scarifications on $(PAH/GO/PAH/PW)_1$ and $(PAH/GO/PAH/PW)_6$ films (Figure S6); detailed optical images and AFM images of the reduced patterns on a $(PAH/GO/PAH/PW)_6$ film (Figure S7). This material is available free of charge via the Internet at http://pubs.acs.org.

■ AUTHOR INFORMATION

Corresponding Author

feng@mpip-mainz.mpg.de; muellen@mpip-mainz.mpg.de; bubeck@mpip-mainz.mpg.de

■ ACKNOWLEDGMENT

This work was financially supported by Alexander von Humboldt Foundation to H.L., and the Max Planck Society through the program ENERCHEM, DFG MU 334/32-1, DFG Priority Program SPP 1459, BMBF Project Graphenoid, BMBF Project LiBZ, ESF Project GOSPEL (ref. no. 09-EuroGRAPHENE-FP-001), EU Project MOLESOL, EU Project GENIUS, and ERC grant on NANOGRAPH. We thank G. Herrmann and W. Scholdei for considerable technical assistance and D. Zheng from Jilin University for XPS measurements.

■ REFERENCES

(1) Novoselov, K. S.; Geim, A. K.; Morozov, S. W.; Jiang, D.; Zhang, Y.; Dubonos, S. W.; Grigorieva, I. V.; Firsov, A. A. *Science* **2004**, *306*, 666–669.
(2) Geim, A. K.; Novoselov, K. S. *Nat. Mater.* **2007**, *6*, 183–191.
(3) Geim, A. K. *Science* **2009**, *324*, 1530–1534.
(4) Dreyer, D. R.; Ruoff, R. S.; Bielawski, C. W. *Angew. Chem. Int. Ed.* **2010**, *49*, 9336–9344.
(5) Cai, J.; Ruffieux, P.; Jaafar, R.; Bieri, M.; Braun, T.; Blankenburg, S.; Muoth, M.; Seitsonen, A. P.; Saleh, M.; Feng, X. L.; Müllen, K.; Fasel, R. *Nature* **2010**, *466*, 470–473.
(6) Schwierz, F. *Nat. Nanotechnol.* **2010**, *5*, 487–496.
(7) Bonaccorso, F.; Sun, Z.; Hasan, T.; Ferrar, A. C. *Nat. Photon.* **2010**, *4*, 611–622.
(8) Zhu, Y.; Murali, S.; Cai, W.; Li, X.; Suk, J. W.; Potts, J. R.; Ruoff., R. S. *Adv. Mater.* **2010**, *22*, 3906–3924.
(9) Dreyer, D. R.; Park, S.; Bielawski, C. W.; Ruoff., R. S. *Chem. Soc. Rev.* **2010**, *39*, 228–240.
(10) Park, S.; Ruoff, R. S. *Nat. Nanotechnol.* **2009**, *4*, 217–224.
(11) Eda, G.; Chhowalla, M. *Adv. Mater.* **2010**, *22*, 2392–2415.
(12) Gilje, S.; Han, S.; Wang, M.; Wang, K. L.; Kaner, R. B. *Nano Lett.* **2007**, *7*, 3394–3398.
(13) Wang, X.; Zhi, L.; Müllen, K. *Nano Lett.* **2008**, *8*, 323–327.
(14) Liang, Y. Y.; Zhi, L. J.; Norouzi-Arasi, H.; Feng, X. L.; Müllen, K. *Nanotechnology* **2009**, *20*, 434007.
(15) Eda, G.; Fanchini, G.; Chhowalla, M. *Nat. Nanotechnol.* **2008**, *3*, 270–274.
(16) Li, D.; Müller, M. B.; Gilje, S.; Kaner, R. B.; Wallace, G. G. *Nat. Nanotechnol.* **2008**, *3*, 101–105.
(17) Decher, G. *Science* **1997**, *277*, 1232–1237.
(18) Fendler, J. H. *Chem. Mater.* **1996**, *8*, 1616–1624.
(19) Hammond, P. T. *Adv. Mater.* **2004**, *16*, 1271–1293.
(20) Kotov, N. A.; Dékány, M.; Fendler, J. H. *Adv. Mater.* **1996**, *8*, 637–641.
(21) Zhao, X.; Zhang, Q.; Hao, Y.; Li, Y.; Fang, Y.; Chen, D. *Macromolecules* **2010**, *43*, 9411–9416.
(22) Williams, G.; Seger, B.; Kamat, P. V. *ACS Nano* **2008**, *2*, 1487–1491.
(23) Williams, G.; Kamat, P. K. *Langmuir* **2009**, *25*, 13869–13873.
(24) Cote, L. J.; Cruz-Silva, R.; Huang, J. *J. Am. Chem. Soc.* **2009**, *131*, 11027–11032.
(25) Manga, K. K.; Zhou, Y.; Yan, Y.; Loh, K. P. *Adv. Funct. Mater.* **2009**, *19*, 3638–3643.
(26) Li, H.; Pang, S.; Feng, X.; Müllen, K.; Bubeck, C. *Chem. Commun.* **2010**, *46*, 6243–6245.
(27) Caruso, F.; Kurth, D. G.; Volkmer, D.; Koop, M. J.; Müller, A. *Langmuir* **1998**, *14*, 3462–3465.
(28) Moriguchi, I.; Fendler, J. H. *Chem. Mater.* **1998**, *10*, 2205–2211.
(29) Ichinose, I.; Tagawa, H.; Mizuki, S.; Lvov, Y.; Kunitake, T. *Langmuir* **1998**, *14*, 187–192.
(30) Kurth, D. G.; Volkmer, D.; Ruttorf, M.; Richter, B.; Müller, A. *Chem. Mater.* **2000**, *12*, 2829–2831.
(31) Liu, S.; Kurth, D. G.; Bredenkötter, B.; Volkmer, D. *J. Am. Chem. Soc.* **2002**, *124*, 12279–12287.
(32) Hummers, W. S.; Offeman, R. E. *J. Am. Chem. Soc.* **1958**, *80*, 1339–1339.
(33) Li, D.; Swanson, B. I.; Robinson, J. M.; Hoffbauer, M. A. *J. Am. Chem. Soc.* **1993**, *115*, 6975–6980.
(34) Keggin, J. F. *Proc. R. Soc. A* **1934**, *144*, 75–100.
(35) Vesel, A.; Mozetic, M.; Zalar, A. *Vacuum* **2008**, *82*, 248–251.
(36) Hiskia, A.; Mylonas, A.; Papaconstantinou, E. *Chem. Soc. Rev.* **2001**, *30*, 62–69.
(37) Li, H.; Yang, Y.; Wang, Y.; Li, W.; Bi, L.; Wu, L. *Chem. Commun.* **2010**, *46*, 3750–3752.
(38) Stankovich, S.; Dikin, D. A.; Piner, R. D.; Kohlhaas, K. A.; Kleinhammes, A.; Jia, Y.; Wu, Y.; Nguyen, S. T.; Ruoff, R. S. *Carbon* **2007**, *45*, 1558–1565.
(39) Eda, G.; Chhowalla, M. *Nano Lett.* **2009**, *9*, 814–818.
(40) Yamaguchi, H.; Eda, G.; Mattevi, C.; Kim, H.; Chhowalla, M. *ACS Nano* **2010**, *4*, 524–528.
(41) Kobayashi, T.; Kimura, N.; Chi, J.; Hirata, S.; Hobara, D. *Small* **2010**, *6*, 1210–1215.
(42) Pang, S.; Tsao, H. N.; Feng, X.; Müllen, K. *Adv. Mater.* **2009**, *21*, 3488–3491.
(43) Yao, P.; Chen, P.; Jiang, L.; Zhao, H.; Zhu, H.; Zhou, D.; Hu, W.; Han, B.; Liu, M. *Adv. Mater.* **2010**, *22*, 5008–5012.
(44) Dennler, G.; Scharber, M. C.; Brabec, C. J. *Adv. Mater.* **2009**, *21*, 1323–1338.
(45) Zhao, J.; Pei, S.; Ren, W.; Gao, L.; Chen, H. *ACS Nano* **2010**, *4*, 5245–5252.
(46) Wang, S.; Ang, P. K.; Wang, Z.; Tang, A. L. L.; Tong, J. T. L.; Loh, K. P. *Nano Lett.* **2010**, *10*, 92–98.
(47) Lehmann, J.; Gaita-arino, A.; Coronad, E.; Loss, D. *Nat. Nanotechnol.* **2007**, *2*, 312–317.
(48) Zhang, H.; Lin, X.; Yan, Y.; Wu, L. *Chem. Commun.* **2006**, 4575–4577.